Medical Engineering and Physics 59 (2018) 50–55

Contents lists available at ScienceDirect

Medical Engineering and Physics

journal homepage: www.elsevier.com/locate/medengphy

On a "Columbus' Egg": Modeling the shape of asymptomatic, dysplastic and impinged hip joints

Daniel Simões Lopes [a,b,*], Sara M. Pires [b], Vasco V. Mascarenhas [c], Miguel T. Silva [b], Joaquim A. Jorge [a,b]

[a] INESC-ID taguspark. Avenida Professor Cavaco Silva, Edifício IST, 2744-016 Porto Salvo, Portugal
[b] Instituto Superior Técnico, Universidade de Lisboa, Av. Rovisco Pais 1, 1049-001 Lisboa, Portugal
[c] Hospital da Luz, UIME, Av. Lusíada 100, 1500-650 Lisboa, Portugal

ARTICLE INFO

Article history:
Received 7 November 2017
Revised 12 June 2018
Accepted 9 July 2018

Keywords:
Hip joint
Femoral head
Acetabular cavity
Femoroacetabular impingement
Hip dysplasia
Surface fitting
Ellipsoid
Ovoid

ABSTRACT

Understanding morphological features that characterize normal hip joint is critical and necessary for a more comprehensive definition of pathological presentations, such as femoroacetabular impingement and hip dysplasia. Based on anatomical observations that articular surfaces of synovial joints are better represented by ovoidal shapes than by spheres, the aim of this study is to computationally test this morphological classification for the femoral head and acetabular cavity of asymptomatic, dysplastic and impinged hips by comparing spherical, ellipsoidal and ovoidal shapes. An image-based surface fitting framework was used to assess the goodness-of-fit of spherical, ellipsoidal and tapered ellipsoidal (i.e., egg-like) shapes. The framework involved image segmentation with active contour methods, mesh smoothing and decimation, and surface fitting to point clouds performed with genetic algorithms. Image data of the hip region was obtained from computed tomography and magnetic resonance imaging scans. Shape analyses were performed upon image data from 20 asymptomatic, 20 dysplastic and 20 impinged (cam, pincer, and mixed) hips of patients with ages ranging between 18 and 45 years old (28 male and 32 women). Tapered ellipsoids presented the lowest fitting errors (i.e., more oval), followed by ellipsoids and spheres which had the worst goodness-of-fit. Ovoidal geometries are also more representative of cam, pincer, mixed impinged hips when compared to spherical or ellipsoidal shapes. The statistical analysis of the surface fitting errors reveal that ovoidal shapes better represent both articular surfaces of the hip joint, revealing a greater approximation to the overall features of asymptomatic, dysplastic and impinged cases.
© 2018 IPEM. Published by Elsevier Ltd. All rights reserved.

1. Introduction

Morphological variations of the hip joint anatomy, such as femoroacetabular impingement (FAI) and dysplasia, have been suggested to be linked to the lesion mechanism of articular cartilage and progress towards osteoarthritis (OA) [1–9]. It has been estimated that FAI morphology affects between 10% and 15% of the general adult population [10] and approximately 55% among young athletes [11]. Regarding hip dysplasia prevalence in adults, it exhibits high variability amongst different racial groups, going from approximately 6–21% [12]. Considering the young age of patients manifesting symptomatic FAI or dysplasia, they might be electable for hip conservative surgery and the application of a prosthetic device [6,13]. An early-stage intervention and appropriate diagnosis for these patients rely on the accurate morphological and geometric characterization of the underlying anatomic deformity [4]. However, consensus regarding the metrics that best identify the morphological deformities and the intervals in which they should be placed to distinguish normal from pathological hips has not been reached to date [3,6,14–17].

Regarding the shape of the hip joint, recent computational tests [18–24] are in line with medical evidence [25,26] which considers that ovoidal shapes represent the articular surface geometry better than the orthodoxal sphere [27,28]. Yet, current tools used by physicians to investigate morphological features of these structures and to guide them in the treatment of FAI and dysplasia, consider the sphere to be the shape that best fits both the femoral head and the acetabular cavity. Consequently, finding how appropriate are currently used 2D quantitative measurements and how well defined is the morphological difference between asymptomatic,

* Corresponding author at: INESC-ID taguspark. Avenida Professor Cavaco Silva, Edifício IST, 2744-016 Porto Salvo, Portugal.
E-mail addresses: daniel.lopes@inesc-id.pt (D.S. Lopes), sara.pires@tecnico.ulisboa.pt (S.M. Pires), vmascarenhas@hospitaldaluz.pt (V.V. Mascarenhas), MiguelSilva@tecnico.ulisboa.pt (M.T. Silva), jorgej@acm.org (J.A. Jorge).

https://doi.org/10.1016/j.medengphy.2018.07.001
1350-4533/© 2018 IPEM. Published by Elsevier Ltd. All rights reserved.

femoroacetabular impingement, and hip dysplasia are interesting questions worth addressing.

On the other hand, there seems to be high variation in the definition of the physiological values for the metrics used to describe the geometry of these surfaces, such as α angle, centre-edge angle, acetabular index of Tönnis, among others. Different authors consider different intervals for these parameters, highlighting the ambiguity associated with the classification of hip joint morphology [6,14–16]. Novel hip joint shape models, along with new sets of parameters, would allow for clear and unambiguous classification and identification of the femoral head and acetabular cavity, regardless of the form.

In order to answer these questions, a comparative study between asymptomatic and pathological hip joints was carried out to understand their underlying morphology. Surface fitting analyses of both femoral head and acetabular cavity were performed upon 20 asymptomatic hips, 20 dysplastic and 20 FAI (cam, pincer, and mixed) hips to provide quantitative evidence supporting the series of anatomical observations that the hip joint exhibits morphological features that are more consistent with ovoidal shapes than spherical ones, given that these do not contain information on global geometric characteristics such as axial asymmetry and non-homogeneous curvature.

2. Materials and methods

2.1. Medical image data

We retrospectively studied adult patients undergoing computed tomography (CT) or magnetic resonance imaging (MRI) from January and December 2015. All eligible patients had completed a questionnaire regarding their clinical history, including current or past hip/groin pain, medical or surgical hip-joint conditions, history of childhood hip pathology, and/or hip trauma. Patients who gave a positive answer to one or more of these questions were excluded from the asymptomatic group. Additionally, all patients completed the non-arthritic hip score questionnaire. Any patient with less than the maximal possible score was also excluded from the asymptomatic cohort. Images were uploaded for analysis using Articulis (ArticulisTM; Clinical Graphics, Delft, The Netherlands) and semi-automatically segmented using this software, which had been previously validated for reliability and accuracy [29].

CT scans of the asymptomatic pelvis (512×512 acquisition matrix, in-plane and resolutions = 0.602–0.869 mm, slice thickness = 1.5–2 mm, 262–929 slices) from 20 individuals with ages between 18 and 45 years (32.9 ± 8.5 years, 9 males and 11 females) were acquired with a Siemens Emotion 16 (Siemens Healthineers, Germany). Patients were positioned in a standard supine position with legs parallel in neutral rotation and received no additional radiation beyond that required for the CT ordered to evaluate their medical condition. The pelvis was reconstructed with 1 mm thickness from the anterosuperior iliac spine to the lesser trochanters. As for symptomatic pelves, MRI scans ((224–256)×(224–256) acquisition matrix, in-plane and resolutions = 0.703–0.804 mm, slice thickness = 0.7–0.8 mm, 96–128 slices) were acquired from 20 individuals with dysplastic hips with ages between 14 and 49 yr (34.0 ± 9.8 years, 6 males and 14 females), and of impinged hips ((224–256)×(224–256) acquisition matrix, in-plane and resolutions = 0.703–0.804 mm, slice thickness = 0.7–0.8 mm, 96–128 slices) from 20 subjects with ages between 21 and 53 yr (38.9 ± 6.8 years, 13 males and 7 females) using a T1-VIBE Fat-suppressed sequence performed by a Siemens MAGNETOM® 3T Verio (Siemens Healthineers, Germany) and an eight-channel body matrix phased-array surface coil (which was placed over the hip of the patient) and a six-channel spine matrix coil (which was integrated in the patient table) were used. As part of the routine MR protocol in patients, a three-dimensional (3D) data set of the whole pelvis was obtained with an axial water excitation true fast imaging with steady-state precession (FISP). MR was performed in standard supine position with legs parallel in neutral rotation. The pelvis was reconstructed with 1 mm thickness slices from the anterosuperior iliac spine to the lesser trochanters. All data sets were anonymized. Informed consent was obtained for the use of the CT and MRI data sets from all subjects.

Cam-type deformities at the femoral head-neck junction were defined as an α angle greater than 55° at any location around the femoral neck [9,30]. Pincer type and acetabular dysplasia were considered if lateral center edge angle was greater than 40° or inferior to 20°, respectively [8,10,12]. Mixed FAI cases had both characteristics of Pincer and CAM cases.

2.2. Surface shapes

Based on results from a previous study that indicates that ellipsoids and egg-like shapes are better suited to fit the femoral head when compared to the sphere shape [23], we adopted the same assumption and considered the following shape models: sphere (S), ellipsoid (E) and tapered ellipsoid (TE). These shapes reveal an increasing degree of complexity to account for as many variations as possible within the set of subjects being considered in the study. The mathematical expressions for the considered shapes (implicit representation) are written as

$$\text{sphere } F_S(x,y,z) = \left(\frac{x}{a}\right)^2 + \left(\frac{y}{a}\right)^2 + \left(\frac{z}{a}\right)^2 \tag{1}$$

$$\text{ellipsoid} \quad F_E(x,y,z) = \left(\frac{x}{a}\right)^2 + \left(\frac{y}{b}\right)^2 + \left(\frac{z}{c}\right)^2 \tag{2}$$

$$\text{tapered ellipsoid} \quad F_{TE}(x,y,z) = \left(\frac{\frac{x}{a}}{T_x z + 1}\right)^2 + \left(\frac{\frac{y}{b}}{T_y z + 1}\right)^2 + \left(\frac{z}{c}\right)^2 \tag{3}$$

where x, y, z are the local coordinates of the point in space that belongs to the surface; a, b, c represent shape dimensions or semi-axis radii; T_x and T_y are the tapering values in the x and y directions.

2.3. Surface fitting and error analysis

The surface fitting framework presented by Lopes et al. [23] was used to reconstruct three-dimensional bone structures from the images and to fit well-defined mathematical surfaces (Fig. 1). Note that all the 3D reconstructed articular surface meshes correspond to the interface between cortical bone and cartilage (i.e., geometric modeling does not take into account soft tissues, merely the outer boundary of bony tissue and not the free surface of the articular surface).

From the medical images, each bone structure is segmented separately using a semi-automatic method that relies on active contour evolution [31] using ITK-SNAP software tools (version 3.4). Afterwards, the resulting segmented images were reconstructed into 3D surface meshes in ParaView (version 4.3.1) with the marching cubes algorithm [32,33]. Since the marching cubes meshes present a characteristic stair-step shape surface and an excessive and redundant amount of vertex information, mesh adjustment operations, namely smoothing and decimation, were then applied to the reconstructed 3D surface meshes, in order to guarantee homogeneous nodal distribution and eliminate these artifacts that result from 3D reconstruction from scanned image data. From the 3-D models, which presented non-articular bony surfaces

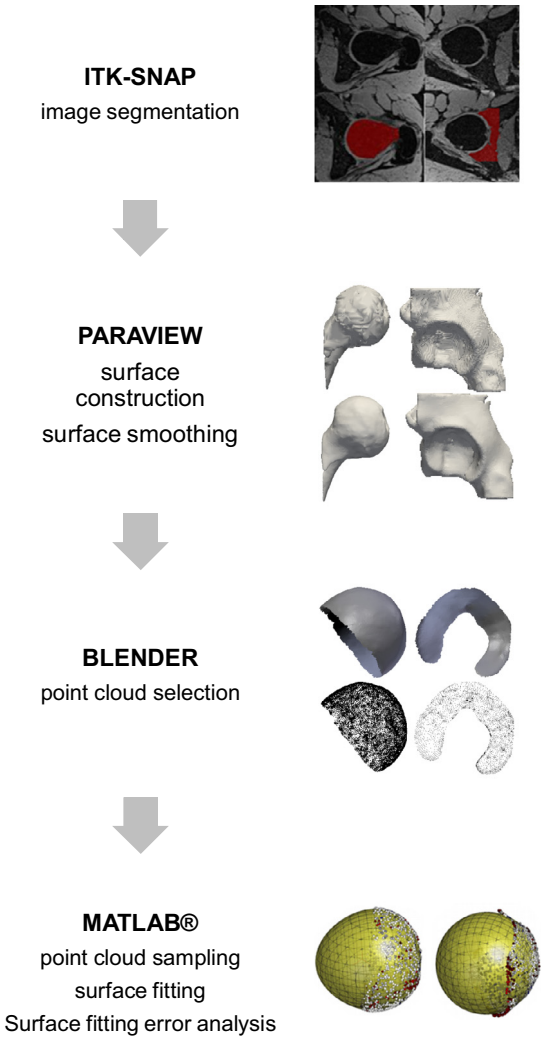

Fig. 1. Image-based surface fitting framework used to extract geometric information of spheroidal articular surfaces of the hip joint. File formats used as input in the software tools consist of DICOM medical images (*.dcm), segmented images (*.mha), triangular surface mesh (*.ply) and point cloud (*.obj).

such as the greater and lesser trochanter, we manually selected the vertices of the articular surfaces and stored them as point clouds using the brush selection tool available on Blender (version 2.75).

In order to identify and characterize the underlying morphology of the point clouds of both femoral head and acetabular cavity, implicit surface shape models (Eqs. 1–3) were adjusted to a cloud of points using a least-squares minimization approach formalized as a nonlinear optimization problem with simple boundary constraints [23]: given a set of points that belong to the outer cortical bone surface, a vector of geometric parameters (i.e., orientation, position, dimension, shape parameters) is determined to minimize the error-of-fit objective function defined as the square sum of residuals, where each residual is the difference between the shape model (Eqs. 1–3) and the corresponding point datum. Due to the non-linearity of the objective function, we approached the minimization problem with a metaheuristic Genetic Algorithm. To guarantee efficient and effective minimizations, close initial approximations in the neighborhood of the global solutions are required. Close initial approximations for sphere and ellipsoid shapes can be obtained by considering a least squares approach with a quadric surface approximation [34], which settles a close approximation of geometric parameters (i.e., position, ellipsoid orientation, sphere radius or ellipsoid radii). To provide a good initial approximation for the tapered ellipsoid, we relied on the observation that a tapered ellipsoid can be obtained by a sequence of morphing operations: an ellipsoid is a rescaled sphere and a tapered ellipsoid is an ellipsoid that lacks a symmetric axis. Thus, the surface fitting process of the tapered ellipsoid was initiated with recourse to the optimal ellipsoid parameters (i.e., position, orientation, radii). It is important to mention that several Genetic Algorithm optimization runs were then carried out to finetune the initial approximation, hence, for every surface fitting case, the optimization algorithm is constrained by boundary constraints, which are defined as simple inequalities affecting the surface parameters and are settled as a set of intervals centered at the good initial approximation and with user-defined limit constants.

Lastly, the comparison between the statistical metrics of goodness-of-fit was assessed according to the surface error, i.e., the signed Euclidean distance of each point in the point clouds to the optimally fitted surface of each shape model, which are computed according to an orthogonal distance optimization framework: points laying on the surface have zero valued distance, points inside the surface have 'negative distances' while points outside have positive valued distances In particular, a statistical analysis was then performed using first-order measures (i.e., mean, standard deviation, minimum and maximum) for each condition and joint structure, whereas paired Student's *t*-test were applied to verify if differences between the surface fitting errors were significant. Both optimization codes were implemented in Matlab® (version R2014a) using the Genetic Algorithm and Direct Search Toolbox™.

3. Results

The statistical analyses of the surface errors for each condition (asymptomatic, FAI, dysplasia) and articular surface (femoral head, acetabular cavity) was performed to quantify the goodness-of-fit of the considered shape models (S, E, TE). The resulting statistical metrics revealed which shape, along with associated shape parameters, best characterizes the general morphological features of the different hip joints.

Through visual inspection, it was possible to perform an initial assessment of the overall goodness-of-fit of the shape models to the femoral head (Fig. 2) and acetabular cavity (Fig. 3). In general, all shape models closely approximated the different anatomical structures. To assist visual inspection, a color map was designed to encode the signed Euclidean distance between each point to the closest point on the approximated surface (Figs. 2–3). Therefore, the point clouds representing the femoral head and acetabular cavity are much better approximated by primitives with less spherical geometric features, being the tapered ellipsoid the most well-adjusted shape.

Regarding the quantitative analysis of surface fitting errors for the three shape models, the statistical assessment relied on the first-order measures (i.e., mean, standard deviation, minimum and maximum) for the whole population of each condition and joint structure (Tables 1–2). The average surface fitting errors followed a similar pattern reported by Lopes et al. [23]: the sphere shape fits worse than its morphological cousins, whereas the ovoidal shape fits best (Table 1-2).

Table 1 - Surface fitting errors statistical analysis of the femoral head for each shape and total number of subjects considered in the study. All metrics are represented in millimeters (mm). The mean and standard deviation are calculated for the absolute value of the surface error. Min and Max values are represented based on the minimal signed Euclidean distances calculated between each point and the optimal fitted shape. (S - Sphere; E - Ellipsoid; TE - Tapered Ellipsoid).

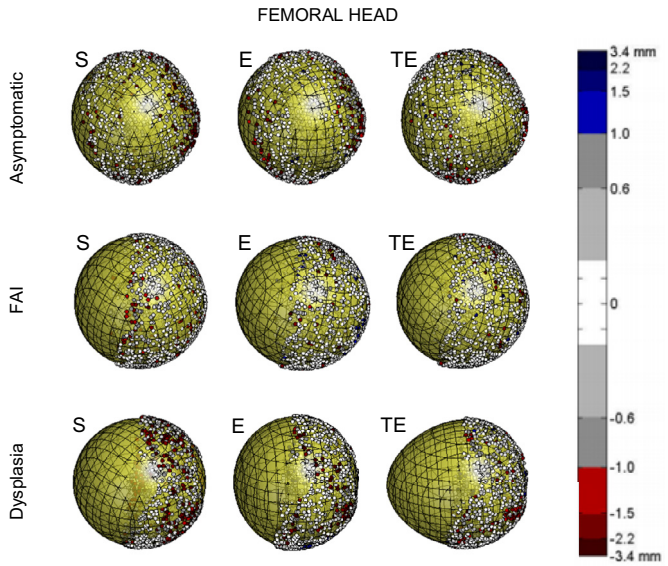

Fig. 2. 3-D view of the optimally fitted surfaces for the femoral head of asymptomatic, FAI and dysplastic hips. Each point cloud corresponds to the femoral head of the first subject of each hip population. Surface error color map: points inside the surface are represented in red; points outside the surface are colored in blue; remaining points whose distance to the surface is between −1.0 mm and 1.0 mm are represented in a gray scale; white corresponds to points with surface errors in the vicinity of 0.0 mm; maximum (+3.4 mm) and minimum (−3.4 mm) surface errors computed for all subjects, shapes, and articular surfaces delimit the color map. (For interpretation of the references to color in this figure legend, the reader is referred to the web version of this article).

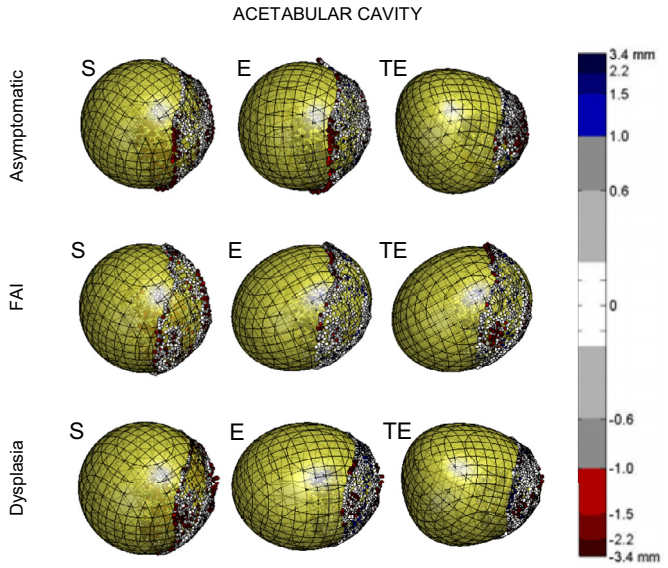

Fig. 3. Fig. 3. 3-D view of the optimally fitted surfaces for the acetabular cavity of asymptomatic, FAI and dysplastic hips. Each point cloud corresponds to the acetabular cavity of the first subject of each hip population. Surface error color map: points inside the surface are represented in red; points outside the surface are colored in blue; remaining points whose distance to the surface is between −1.0 mm and 1.0 mm are represented in a gray scale; white corresponds to points with surface errors in the vicinity of 0.0 mm; maximum (+3.4 mm) and minimum (−3.4 mm) surface errors computed for all subjects, shapes, and articular surfaces delimit the color map. (For interpretation of the references to color in this figure legend, the reader is referred to the web version of this article).

Table 1
Surface fitting errors statistical analysis of the femoral head for each shape and total number of subjects considered in the study. All metrics are represented in millimeters (mm). (S - Sphere; E - Ellipsoid; TE - Tapered Ellipsoid).

Femoral head					
Type	# Subjects		S	E	TE
Asymptomatic	20	μ	0.653	0.591	0.538
		σ	0.575	0.544	0.520
		Min	−3.464	−2.857	−2.831
		Max	1.592	3.464	3.464
FAI	20	μ	0.521	0.458	0.414
		σ	0.476	0.445	0.418
		Min	−3.464	−3.426	−2.874
		Max	-2.7×10^{-5}	2.787	2.892
FAI (cam)	7	μ	0.534	0.479	0.431
		σ	0.489	0.449	0.425
		Min	−3.461	−3.426	−2.874
		Max	-4.4×10^{-5}	2.787	2.672
FAI (pincer)	6	μ	0.515	0.478	0.429
		σ	0.450	0.443	0.415
		Min	−2.702	−2.624	−2.293
		Max	-4.1×10^{-5}	2.191	2.405
FAI (mixed)	7	μ	0.512	0.419	0.385
		σ	0.485	0.440	0.413
		Min	−3.464	−3.178	−2.718
		Max	-2.7×10^{-5}	2.525	2.892
Dysplasia	20	μ	0.578	0.459	0.449
		σ	0.485	0.434	0.430
		Min	−2.850	−2.806	−2.698
		Max	2.500	2.776	2.621

Table 2
Surface fitting errors statistical analysis of the acetabular cavity for each shape and total number of subjects considered in the study. All metrics are represented in millimeters (mm). (S - Sphere; E - Ellipsoid; TE - Tapered Ellipsoid).

Acetabular cavity					
Type	# Subjects		S	E	TE
Asymptomatic	20	μ	0.789	0.640	0.611
		σ	0.552	0.508	0.491
		Min	−3.464	−3.458	−3.449
		Max	-3.0×10^{-5}	2.789	2.943
FAI	20	μ	0.742	0.606	0.570
		σ	0.524	0.479	0.467
		Min	−3.240	−2.980	−2.726
		Max	2.301	2.612	2.600
FAI (cam)	7	μ	0.773	0.631	0.592
		σ	0.542	0.497	0.476
		Min	−3.146	−2.980	−2.684
		Max	2.301	2.612	2.600
FAI (pincer)	6	μ	0.653	0.547	0.525
		σ	0.482	0.450	0.447
		Min	−2.774	−2.711	−2.726
		Max	0.685	2.317	2.476
FAI (mixed)	7	μ	0.788	0.632	0.587
		σ	0.531	0.480	0.474
		Min	−3.240	−2.827	−2.622
		Max	-6.9×10^{-5}	2.473	2.538
Dysplasia	20	μ	0.740	0.602	0.580
		σ	0.536	0.488	0.485
		Min	−3.432	−2.921	−3.001
		Max	0.834	2.734	2.605

Table 2 - Surface fitting errors statistical analysis of the acetabular cavity for each shape and total number of subjects considered in the study. The mean and standard deviation are calculated for the absolute value of the surface error. Min and Max values are represented based on the minimal signed Euclidean distances calculated between each point and the optimal fitted shape. All metrics are represented in millimeters (mm). (S - Sphere; E - Ellipsoid; TE - Tapered Ellipsoid).

Table 3
The p-values relative to the statistical significance of the differences between fitting errors for all shape models for the femoral head and acetabular cavity, using a paired Student *t*-test with statistical significance set at $p < 0.05$. (S - Sphere; E - Ellipsoid; TE - Tapered Ellipsoid).

	Femoral head		Acetabular cavity	
Asymptomatic	S ↔ E	0.000	S ↔ E	0.000
	S ↔ TE	0.000	S ↔ TE	0.609
	E ↔ TE	0.000	E ↔ TE	0.000
FAI	S ↔ E	0.000	S ↔ E	0.000
	S ↔ TE	0.000	S ↔ TE	0.000
	E ↔ TE	0.005	E ↔ TE	0.011
Dysplasia	S ↔ E	0.000	S ↔ E	0.000
	S ↔ TE	0.000	S ↔ TE	0.000
	E ↔ TE	0.005	E ↔ TE	0.123

Relatively to the femoral head, the paired Student's *t*-test used to corroborate the significance of the statistical analysis revealed that the differences between the surface fitting parameters of all pairs of shapes for all conditions were significant (p-value < 0.05) between sphere ↔ ellipsoid, sphere ↔ tapered ellipsoid and also ellipsoid ↔ tapered ellipsoid shapes for all conditions (Table 3). Regarding the statistical significance of the differences in surface fitting errors for the acetabular cavity, in the asymptomatic case, these were significant for the pairs sphere ↔ ellipsoid and ellipsoid ↔ tapered ellipsoid. The pair ellipsoid ↔ tapered ellipsoid presented no statistically significant difference. For the population presenting FAI, the pairs which presented statistical significance were sphere ↔ ellipsoid and sphere ↔ tapered ellipsoid. Finally, subjects with dysplatic hips revealed statistical significance between the surface fitting errors of two pairs of shape models, sphere ↔ ellipsoid and sphere ↔ ellipsoid, while the pair of shapes ellipsoid ↔ tapered ellipsoid exhibited no statistically significant difference.

4. Discussion

The conducted morphological study revealed that the adjustment of the spherical shape to the two articular surfaces to be the worst among the hierarchy of shape models, regardless of the clinical case. On the other hand, ovoidal shapes approximated well not only to the femoral head but also to the acetabular cavity, thus validating MacConaill's assumption for synovial joint classification [25]. Results regarding the geometric parameters of the best-approximated surfaces and the surface fitting errors were considered reliable, given that their order of magnitude was identical to results from other morphological studies of the hip joint [19–23]. This work allowed the comparison of two conditions, revealing that, in general, articular surfaces of hip joints presenting femoroacetabular impingement approximated better to the tapered ellipsoidal shape than dysplastic hips.

Transversal to all three conditions and articular joint surfaces, the following pattern of decreasing surface fitting error arises (i.e., from spherical to ovoidal): $S > E > TE$. Regarding the considered hip conditions for both femoral head and acetabular cavity, asymptomatic hips have a lesser goodness-of-fit than dysplastic and impinged hips. The FAI presenting population obtained the lowest values of average values of the surface fitting errors for the sphere and tapered ellipsoid models. The lowest fitting error belonged to the fitting of the tapered ellipsoid to the FAI presenting population. The dysplastic population followed the same pattern, as did the asymptomatic, which presented the highest fitting errors of the three. A careful look into the average error values shows that dysplastic hips revealed better approximation to all the geometric primitives than the two remaining populations. In the acetabular case, the population for which the lowest fitting errors were obtained was the FAI diagnosed one, which is compliant with the results already seen for the femoral case. Similarly, the shape that fitted the point clouds better for all sets of subjects was the tapered ellipsoid. Therefore, the main novelty of this work consists of introducing shapes with axial asymmetry into morphological studies of asymptomatic, impinged and dysplastic hips. In addition, both articular surfaces of the hip joint were considered.

The major limitation of this work is that more data sets are required to provide a greater statistical significance; in particular an equitative number of FAI cases is required to promote a more fair comparison between cam, pincer, and mixed hips. Nevertheless, the surface fitting error results are at par with other morphology studies which consider non-spherical shapes to better represent femoral and acetabular joint components [19–23]. More importantly, these results question the usefulness of traditional metrics (e.g., α angle, center-edge angle, acetabular index of Tönnis), which describe hip geometry based on the bi-dimensional shapes (i.e., center-side of Wiberg assumes that the femoral head is circular), the systematic errors introduced when performing bi-dimensional measurements could be greater than errors produced by more reliable surface fitting methods based on ovoidal shapes. As future work, ovoidal shapes may also inspire software tools to support ovoidal shape metrics to fabricate personalized endoprosthesis with ovoidal shapes with subject-specific dimensions and curvatures. In addition, we expect to extend the surface fitting framework to also incorporate cartilage surface as this could lead towards new and interesting questions regarding the correlation between cartilaginous surface and bony surface, namely, If cartilage thickness compensates the lack of bony asphericity or simply follows the underlying bony shape, and if this hypothetic correlation is consistent between healthy and unhealthy hips.

Conflicts of interest

Competing interests: None declared.

Ethical approval

This study was approved by the Ethics Research Committee of the Nova Medical School | Faculdade de Ciências Médicas da Universidade Nova de Lisboa (CEFCM) under the Project entitled "DEFORMIDADES COXO-FEMURAIS E CONFLITO FEMUROACETABULAR: contributo epidemiológico, diagnóstico e prognóstico" with reference nr.61/2014/CEFCM.

Acknowledgments

All authors are thankful for the financial support given by Portuguese Foundation for Science and Technology (FCT). In particular, the first author thanks for the postdoctoral grant SFRH/BPD/97449/2013. This work was also partially supported by national funds through FCT with reference UID/CEC/50021/2013 and IT-MEDEX - PTDC/EEI-SII/6038/2014.

Reference

[1] Zeng W-N, Wang F-Y, Chen C, Zhang Y, Gong XY, Zhou K, et al. Investigation of association between hip morphology and prevalence of osteoarthritis. Sci Rep 2016;6:23477.
[2] Ganz R, Parvizi J, Beck M, Leunig M, Nötzli H, Siebenrock KA. Femoroacetabular impingement: a cause for osteoarthritis of the hip. Clin Orthop Relat Res 2003;417:112–20.
[3] Gosvig KK, Jacobsen S, Palm H, Sonne-Holm S, Magnusson E. A new radiological index for assessing asphericity of the femoral head in cam impingement. Bone Joint J 2007;89(10):1309–16.
[4] Peters CL, Erickson JA, Anderson L, Anderson AA, Weiss J. Hip-preserving surgery: understanding complex pathomorphology. J Bone Joint Surg Am 2009;91(Supplement 6):42–58.

[5] Laborie LB, IØ Engesæter, Lehmann TG, Sera F, Dezateux C, Engesæter LB, et al. Radiographic measurements of hip dysplasia at skeletal maturity—new reference intervals based on 2,038 19-year-old Norwegians. Skeletal Radiol 2013;42(7):925–35.
[6] Jorge JP, Simões FMF, Pires EB, Rego PA, Tavares DG, Lopes DS, et al. Finite element simulations of a hip joint with femoroacetabular impingement. Comput Methods Biomech Biomed Eng 2014;17(11):1275–84.
[7] Tannast M, Hanke MS, Zheng G, Steppacher SD, Siebenrock KA. What are the radiographic reference values for acetabular under-and overcoverage? Clin Orthop Relat Res 2015;473(4):1234–46.
[8] Mascarenhas VV, Rego P, Dantas P, Morais F, McWilliams J, Collado D, et al. Imaging prevalence of femoroacetabular impingement in symptomatic patients, athletes, and asymptomatic individuals: a systematic review. Eur J Radiol 2015;85(1):73–95.
[9] Mascarenhas VV, Rego P, Dantas P, Gaspar A, Soldado F, Consciência JG. Cam deformity and the omega angle, a novel quantitative measurement of femoral head-neck morphology: a 3D CT gender analysis in asymptomatic subjects. Eur Radiol 2017;27(5):2011–23.
[10] Laborie LB, Lehmann TG, Engesæter IØ, Eastwood DM, Engesæter LB, Rosendahl K. Prevalence of radiographic findings thought to be associated with femoroacetabular impingement in a population-based cohort of 2081 healthy young adults. Radiology 2011;260(2):494–502.
[11] Frank JM, Harris JD, Erickson BJ, Slikker W, Bush-Joseph CA, Salata MJ, et al. Prevalence of femoroacetabular impingement imaging findings in asymptomatic volunteers: a systematic review. Arthroscopy 2015;31(6):1199–204.
[12] Loder RT, Skopelja EN. The epidemiology and demographics of hip dysplasia. ISRN Orthop 2011;2011:238607.
[13] Clohisy JC, Carlisle JC, Beaulé PE, Kim YJ, Trousdale RT, Sierra RJ, et al. A systematic approach to the plain radiographic evaluation of the young adult hip. J Bone Joint Surg Am 2008;90(Suppl. 4):47–66.
[14] Chegini S, Beck M, Ferguson SJ. The effects of impingement and dysplasia on stress distributions in the hip joint during sitting and walking: a finite element analysis. J Orthop Res 2009;27(2):195–201.
[15] Gerhardt MB, Romero AA, Silvers HJ, Harris DJ, Watanabe D, Mandelbaum BR. The prevalence of radiographic hip abnormalities in elite soccer players. Am J Sports Med 2012;40(3):584–8.
[16] Ng KG, Lamontagne M, Labrosse MR, Beaulé PE. Hip joint stresses due to cam–type femoroacetabular impingement: a systematic review of finite element simulations. PLoS One 2016;11(1):e0147813.
[17] Rego PRA, Mascarenhas V, Oliveira FS, Pinto PC, Gaspar A, Ovídio J, et al. Morphologic and angular planning for cam resection in femoro-acetabular impingement: value of the omega angle. Int Orthop 2016;40(10):2011–17.
[18] Harris MD, Reese SP, Peters CL, Weiss JA, Anderson AE. Three-dimensional quantification of femoral head shape in controls and patients with cam-type femoroacetabular impingement. Ann Biomed Eng 2013;41(6):1162–71.
[19] Cerveri P, Manzotti A, Baroni G. Patient-specific acetabular shape modelling: comparison among sphere, ellipsoid and conchoid parameterisations. Comput Methods Biomech Biomed Eng 2014;17(5):560–7.
[20] Gu D, Chen Y, Dai K, Zhang S, Yuan J. The shape of the acetabular cartilage surface: a geometric morphometric study using three-dimensional scanning. Med Eng Phys 2008;30(8):1024–31.
[21] Liu B, Hua S, Zhang H, Liu Z, Zhao X, Zhang B, et al. A personalized ellipsoid modeling method and matching error analysis for the artificial femoral head design. Comput Aided Des 2014;56:88–103.
[22] Liu B, Zhang H, Hua S, Jiang Q, Huang R, Liu W, et al. An automatic segmentation system of acetabulum in sequential CT images for the personalized artificial femoral head design. Comput Methods Programs Biomed 2015;127:318–35.
[23] Lopes DS, Neptune RR, Gonçalves AA, Ambrósio JA, Silva MT. Shape analysis of the femoral head: a comparative study between spherical, (Super) ellipsoidal, and (Super) ovoidal shapes. J Biomech Eng 2015;137(11):114504.
[24] Menschik F. The hip joint as a conchoid shape. J Biomech 1997;30(9):971–3.
[25] MacConaill MA. A structuro-functional classification of synovial articular units. Ir J Med Sci 1973;142(1):19–26.
[26] Standring S. Gray's anatomy: the anatomical basis of clinical practice. 41st Ed. Elsevier; 2016.
[27] Rouvière H, Delmas A. Anatomía humana: descriptiva, topográfica y funcional. 11th Ed. Barcelona: Masson; 2005.
[28] Williams GM, Chan EF, Temple-Wong MM, Bae WC, Masuda K, Bugbee WD, et al. Shape, loading, and motion in the bioengineering design, fabrication, and testing of personalized synovial joints. J Biomech 2010;43(1):156–65.
[29] Röling MA, Visser MI, Oei EH, Pilot P, Kleinrensink G-J, Bloem RM. A quantitative non-invasive assessment of femoroacetabular impingement with CT-based dynamic simulation cadaveric validation study. BMC Musculoskelet Disord 2015;16:50.
[30] Sutter R, Dietrich TJ, Zingg PO, Pfirrmann CWA. How useful is the alpha angle for discriminating between symptomatic patients with cam–type femoroacetabular impingement and asymptomatic volunteers? Radiology 2012;264(2):514–21.
[31] Yushkevich PA, Piven J, Hazlett HC, Smith RG, Ho S, Gee JC, et al. User-guided 3D active contour segmentation of anatomical structures: significantly improved efficiency and reliability. Neuroimage 2006;31(3):1116–28.
[32] Lorensen WE, Cline HE. Marching cubes: a high resolution 3D surface construction algorithm. In ACM SIGGRAPH Comput Graph 1987;21(4):163–9.
[33] Ahrens J, Geveci B, Law C. 36 Paraview: An end user tool for large-data visualization. In: Hansen Charles D, Johnson Chris R, editors. The Visualization Handbook. Elsevier; 2005. p. 717–31.
[34] Dai M, Newman TS. Hyperbolic and parabolic quadric surface fitting algorithms: comparison between the least squares approach and the parameter optimization approach; 2008. UAH CS Technical Report.